



Contact and macroscopic ageing in colloidal suspensions

Francesco Bonacci¹, Xavier Chateau¹✉, Eric M. Furst², Jennifer Fusier¹, Julie Goyon¹ and Anaël Lemaître¹ ✉

The ageing behaviour of dense suspensions or pastes at rest is almost exclusively attributed to structural dynamics. Here, we identify another ageing process, contact-controlled ageing, consisting of the progressive stiffening of solid–solid contacts of an arrested colloidal suspension. By combining rheometry, confocal microscopy and particle-scale mechanical tests using laser tweezers, we demonstrate that this process governs the shear-modulus ageing of dense aqueous silica and polymer latex suspensions at moderate ionic strengths. We further show that contact-controlled ageing becomes relevant as soon as Coulombic interactions are sufficiently screened out that the formation of solid–solid contacts is not limited by activation barriers. Given that this condition only requires moderate ion concentrations, contact-controlled ageing should be generic in a wide class of materials, such as cements, soils or three-dimensional inks, thus questioning our understanding of ageing dynamics in these systems.

Dense colloidal suspensions (or pastes) constitute a broad class of materials found in areas ranging from environmental systems (for example, silts, clays), to industry (ceramics, drilling muds, slurries) and construction (plaster, cements), foodstuff, cosmetics, pharmaceuticals (toothpaste, medical ceramics). Their most remarkable feature is thixotropy: a slow evolution of mechanical properties when switching between rest and flow (at fixed density, in the absence of drainage)^{1–7}. Under flow, their viscosity depends on time and strain history; at rest, their shear modulus and yield stress often display ageing, that is slow, non-exponential long time dynamics.

In recent decades, tremendous progress has been made towards understanding the dynamics of so-called ‘stabilized’ suspensions, in which the formation of interparticle adhesive contacts is fully avoided by tuning interparticle interactions (especially double-layer polarization); in such cases, only moderate levels of attraction may be introduced; for example, via polymer depletion effects^{8–12}. Confocal microscopy was instrumental to these advances, yet may only be applied to transparent, index matched, systems, in which van der Waals forces are essentially absent. Meanwhile, studies of ‘non-stabilized’ suspensions have focused on very dilute systems (packing fractions at most a few percent) where a structural evolution (floc formation) could be imaged and thus analysed using, for example, light scattering^{13–15}.

The success of these studies has created an observational bias, as classical works on suspensions and recent theoretical approaches only consider structural dynamics as a possible cause of thixotropy^{16–19}. But the pastes of civil and environmental engineering are dense and generally contain sufficient ion concentrations to screen Coulombic repulsion, thus allowing attractive van der Waals forces to bring particles into solid–solid contact, which may strongly influence macroscopic properties and their evolution. Indeed, solid–solid friction, which is time-dependent^{20–22}, is known to affect the macroscopic response of non-colloidal granular materials; the formation of hydrate gels between grains^{23,24} was proposed to play a role in thixotropy²⁵, and contact ageing²⁶ was proposed to be at work in highly

dilute (0.02%) gels of nanometric particles in microgravity—a system far from real pastes. Yet, a direct relation between contact and macroscopic ageing in an attractive suspension has never been established.

In fact, it remains unclear how solid–solid contacts may affect the elastic modulus of colloidal systems. By designing an optical-trap three-point bending test, Pantina and Furst^{27,28} showed that beams of poly-methyl methacrylate (PMMA) and polystyrene particles present a finite flexural modulus, which entails interparticle contacts resisting sliding and rolling. The flexural modulus of polystyrene particle rods was later shown to evolve²⁹. These two findings lead us to ask whether the evolution of the contact bending stiffness could be responsible for mechanical ageing in pastes.

In this work, using rheometry we measure the shear modulus of dense hydrophilic silica suspensions flocculated by the addition of moderate concentrations of a divalent salt. We find that, for suspensions of particles of various sizes (from 0.5 to 1.9 μm), at volume fractions between 29 and 40%, the macroscopic shear modulus G' grows quasi-logarithmically at late times, whereas the microstructure is rapidly frozen. Using laser tweezers, we perform three point-flexural tests on 1.9 μm silica particle beams, at the same salt concentrations. We demonstrate that, in these conditions: (1) silica particles form irreversible solid–solid, roll-resistant contacts; and (2) the contact bending rigidity grows quasi-logarithmically, such as G' , and with the same characteristic timescale. Experimental details are provided in Methods.

These observations lead us to attribute macroscopic ageing, in this system, to the progressive stiffening of contacts in the absence of any structural evolution. A scaling relation identified on this premise permits us to quantitatively reconstruct all of our macroscopic shear modulus data (different particle sizes) from flexural data for a single particle size. This remarkable agreement strongly supports that the growing macroscopic shear modulus is essentially determined by bending (as opposed to elongational) contact rigidity^{30,31}. Similar observations in flocculated dense suspensions of 3 μm PMMA particles support the genericity of contact-driven macroscopic ageing in dense flocculated suspensions.

¹Navier, Ecole des Ponts, Univ Gustave Eiffel, CNRS, Marne-la-vallée, France. ²Department of Chemical and Biomolecular Engineering, University of Delaware, Newark, DE, USA. ✉e-mail: xavier.chateau@enpc.fr; anael.lemaitre@ifsttar.fr

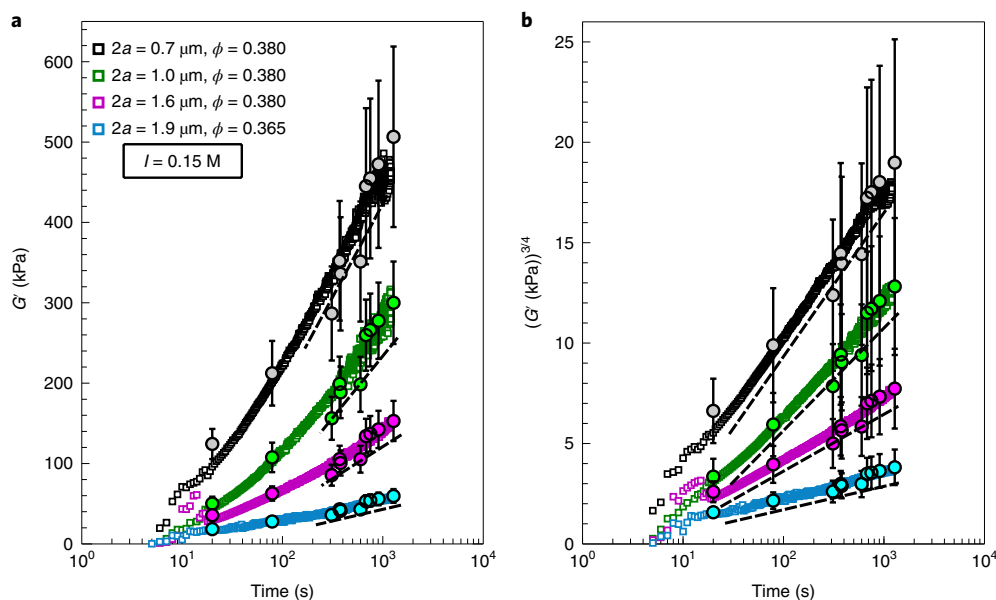


Fig. 1 | Mechanical ageing in dense silica suspensions. The shear modulus G' (squares) as a function of ageing time, for suspensions of ionic strength $I = 0.15 \text{ M}$, for: (1) packing fraction $\phi \approx 38\%$ and particle diameters, $2a = 0.7$ (black), 1 (green) and $1.6 \mu\text{m}$ (purple); (2) $\phi \approx 36.5\%$ and $2a \approx 1.9 \mu\text{m}$ (blue). Filled circles (in lighter corresponding colours) are the predictions obtained by reconstructing (see text) $G'(t)$ using our three-point bending tests (three rod samples). **a**, log-linear plot of G' versus t showing the near logarithmic growth (asymptotes in dashed lines). **b**, log-linear plot of $G'^{3/4}$ versus t supporting the asymptotic scaling $G' \approx (\log(t/\tau))^{4/3}$ (see text for details).

Ageing without microstructural evolution

Before any macroscopic ageing measurement (see Methods), to ensure reproducibility our suspensions are brought into a well-defined initial state via a strong preshearing. Ageing time t is counted starting when the preshearing torque is set to zero. This is a slight overestimate, as a modest rotation of the inner cylinder continues for about 5 s; however, the shear modulus G' is barely measurable until $t \approx 10 \text{ s}$.

As seen in Fig. 1, G' increases monotonically over the accessible time range and reaches asymptotically a quasi-logarithmic growth regime. Its magnitude decreases with the increasing particle radius a . Our $G'(t)$ data also include different packing fractions ϕ , and ionic strengths I : as shown in Supplementary Note 1, G' is essentially I -independent⁷ and strongly increases with ϕ . Meanwhile, it is at least a decade larger than the loss modulus, which establishes the solid-like character of our systems.

To assess whether ageing results from microstructural changes, it would be desirable to image particles, inside our suspensions, using a confocal microscope. Unfortunately, the strong index mismatch between silica ($n \approx 1.5$) and pure water ($n \approx 1.33$) precludes doing so beyond a few particle layers inside the system.

To gain insight on the relevance, or lack thereof, of structural evolution, we have examined suspensions of silica particles in 60/40 wt% water and glycerol mixtures. Supplementary Note 1 shows that these systems present the same quasi-logarithmic shear-modulus ageing as pure water suspensions, albeit of a smaller amplitude. Fig. 2a shows a typical confocal microscopy image at depth of around $15 \mu\text{m}$ in a water-glycerol system. Since $2a = 1.6 \mu\text{m}$, this is deep enough to avoid wall effects. In Fig. 2b, we draw the particle positions reconstructed from this and later images, at three different times in the macroscopic ageing regime. The disappearance of certain particles with time is an effect of the progressive bleaching of the fluorescein—those particles slightly further away from the focal plane become increasingly difficult to distinguish. All the particles that can be imaged at the three considered times essentially remain fixed at the same positions: the microstructure is constant during mechanical ageing.

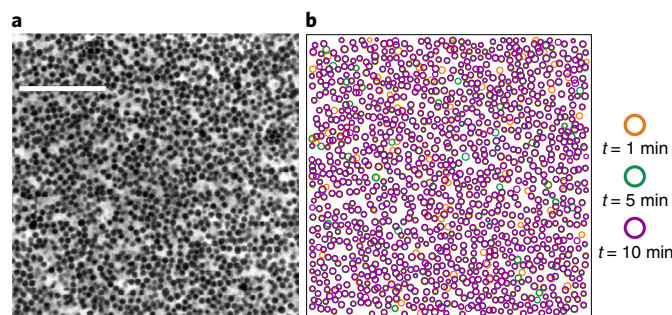


Fig. 2 | Absence of structural ageing in a water-glycerol mixture.

a, Typical confocal image of a suspension of $2a = 1.6 \mu\text{m}$ silica particles in a 60/40 wt% water-glycerol mixture, with $\phi = 39\%$, $I = 0.15 \text{ M}$, in a plane parallel to the bottom coverslip, at a depth of around $15 \mu\text{m}$. Scale bar, $20 \mu\text{m}$. **b**, Reconstructed particle positions at $t = 1$ (orange), 5 (green) and 10 min (purple) after the sample was strongly presheared and destructured manually with a spatula.

These observations establish that, in our silica suspensions in a water-glycerol mixture, shear-modulus ageing proceeds without structural evolution, which suggests that solid-solid contacts are rapidly formed and age. In all likelihood, the same applies to silica particle suspensions in pure water, since van der Waals forces are much larger, hence particles are more likely to form stable solid-solid contacts. This idea is also indirectly supported by the fact that, despite the density mismatch, sedimentation rapidly stops after cessation of preshearing⁷. It leads us to ask two questions:

1. Can we provide evidence for solid-solid contact formation and ageing for silica particles in pure water at relevant ionic strengths?
2. If so, can we predict mechanical ageing from contact ageing, by assuming that the microstructure is rapidly fixed after arrest?

Solid–solid contact stability and ageing

To address question (1), we carry out optical tweezer experiments using Pantina and Furst's method^{27,28}, which consists of assembling an odd number of particles into a rod and performing three-point bending tests, as illustrated in Fig. 3a. This experiment uses particles of diameter $2a = 1.9 \mu\text{m}$ (see Methods for the setup and rod assembly protocol).

In low-ionic-strength aqueous suspensions, electrostatic repulsion³² gives rise to a potential barrier that limits the formation of solid–solid interparticle contacts. A shallow secondary minimum then permits the formation of weak interparticle bonds, that can be broken using optical traps^{33,34}. In Supplementary Note 2 and Supplementary Video we show that here, in contrast:

1. For $I \geq 0.1 \text{ M}$, no repulsive barrier exists to limit contact formation.
2. Consistently, when two particles are approached, they form a contact that resists opening.

In addition,

3. Once formed, rods remain stable for hours when held by just two traps acting on the end particles.

Under the studied conditions, when two particles are approached, they form solid–solid contacts that do not break by thermal activation over the timescale at which we observe macroscopic ageing.

By analysing rod images during the laser-tweezer experiment (see Supplementary Methods), we access the bending force f as a function of rod deflection δ . Typical data for a single rod at different times after its formation are reported in Fig. 3b. Such experiments, replicated at different ionic strengths between 0.10 and 0.20 M, yield the following observations:

4. Under loading, rods bend according to the Euler–Bernoulli equation (see Supplementary Methods and refs. ^{27,28}), which demonstrates that contacts resist rolling.
5. The bending modulus grows over time (Fig. 3b).

Point (4) indicates that the rod stiffness can be characterized by an effective single-bond rigidity,

$$k_0 = k_b \times \left(\frac{L}{a}\right)^3 \quad (1)$$

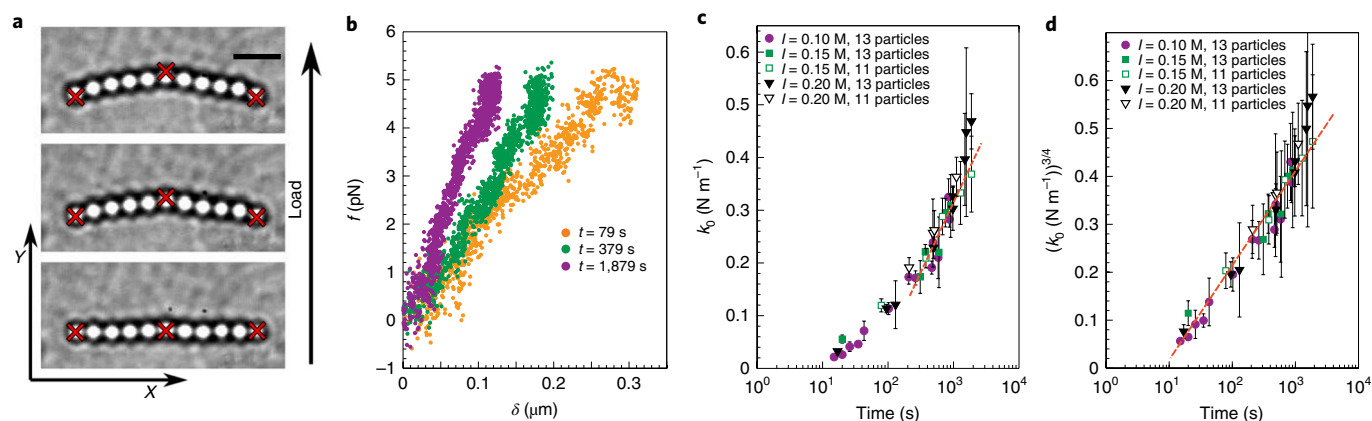


Fig. 3 | Laser-tweezer bending test. **a**, Three snapshots of an 11-particle beam at different loading levels during the three-point bending test; the red crosses schematically represent the positions of optical traps. Scale bar, $5 \mu\text{m}$. **b**, Force f versus beam deflection δ after three ageing times. **c**, Bond stiffness k_0 as a function of time t for different ionic strengths, as measured from three-point bending tests with two rod lengths L (error bars show the confidence interval of the linear fit of f versus δ data). **d**, log-linear plot of $k_0^{3/4}$ versus t supporting that asymptotic growth scales as $\simeq (\log(t/\tau))^{4/3}$ (see text for details).

where L is the rod length and k_b , the rod bending modulus deduced from the Euler–Bernoulli equation. Plotting k_0 versus t for both 11 and 13 particle rods (Fig. 3c) confirms that k_0 is independent of L , and demonstrates that:

6. flexural rigidity reaches a roughly logarithmic growth regime at later times.

Like $G'(t)$, $k_0(t)$ shows an upward curve, so that the logarithmic scaling extends over less than a decade.

Also, k_0 is I -independent at the considered salt concentrations: this expectedly results from the saturation, for $I \geq 0.1 \text{ M}$, of the zeta potential (at $\cong -10 \text{ mV}$), hence of the charge density, of our particles (see ref. ⁷ and Supplementary Note 2).

Two key conclusions may be drawn from these observations. First, points (1)–(4) demonstrate the non-barrier-limited formation of solid–solid, roll-resistant, contacts that do not break by thermal activation. This unambiguously supports that the rapid formation of contacts stabilizes suspension microstructures shortly after arrest. Second, the evolution of the effective flexural rigidity of rods demonstrates that solid–solid interparticle contacts age.

From contact to macroscopic ageing

This now brings us to the original question (2). For a fixed microstructure, we expect

$$G'(t) = \frac{S}{a} \times k_0(t) \quad (2)$$

with S , a t -independent dimensionless quantity, characterizing the structure. This linear relation is indeed clearly supported by plotting $G'(t)$ versus $k_0(t)$ for our $2a \cong 1.9 \mu\text{m}$ particles (blue symbols in Fig. 4a); it also applies to all the studied ionic strengths and packing fractions. These data show that, in the tested conditions, macroscopic ageing results from the progressive stiffening of interparticle contacts, the microstructure being essentially frozen shortly after arrest.

Let us explore in more detail the possible origin of contact ageing and its consequences in terms of macroscopic ageing. We recall that interparticle solid–solid contacts are flat circular areas of radius

$$a_c = A \left(\frac{3\pi a^2 W}{8E^*}\right)^{1/3} \quad (3)$$

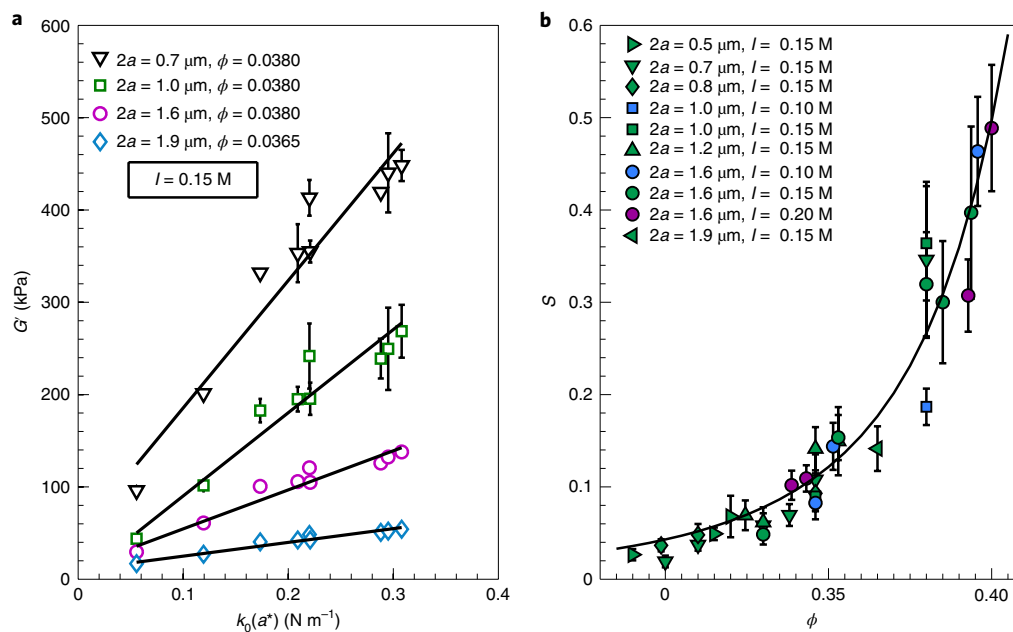


Fig. 4 | Matching microscopic and macroscopic data. **a**, The macroscopic shear modulus $G'(t)$ for four particle sizes versus the effective flexural rigidity $k_0(a^*; t)$ at the same ageing time t , where $2a^* = 1.9 \mu\text{m}$; error bars show the standard deviation of G' data over centred 5-s intervals. **b**, Structural parameter S as a function of packing fraction ϕ for different particle sizes (symbols) and ionic strengths (colours) and the curve $S = S_0/(\phi_c - \phi)^\alpha$ with $\phi_c \simeq 0.52$ and $\alpha = 4$ (solid line). The error bars show the confidence interval of the G' versus k_0 linear fit.

where A is a prefactor ranging from 1 to $\sim 3^{1/3} = 1.44$ between the Derjaguin–Muller–Toporov (DMT) and Johnson–Kendall–Roberts (JKR) limits^{35–37}. For Stöber silica, as Young’s modulus $E \approx 30 \text{ GPa}$ and Poisson’s ratio $\nu \simeq 0.17$ (ref. ³⁸), the reduced modulus $E^* = E/(1 - \nu^2)/2 \simeq 15 \text{ GPa}$. For a freshly formed contact, the surface energy $W \simeq 2 \gamma_{SL}$ with γ_{SL} as the silica–water interfacial energy, which ranges between 50 and 100 mJ m^{-2} (ref. ³⁹). The Tabor number $\lambda = (W^2 a / (8(E^*)^2 h^3))^{1/3}$, where h is the gap (contact thickness), is small in the DMT limit and large in the JKR one. It may be bounded above provided $W \lesssim 200 \text{ mJ m}^{-2}$, by taking $2a \simeq 1.9 \mu\text{m}$, an upper limit for the particle diameter and $h \simeq 0.3 \text{ nm}$, a lower value for the gap⁴⁰. Therefore, $\lambda \lesssim 0.9$, which leads us to use the DMT estimate $A \simeq 1$ throughout. The ensuing analysis will support that contact stiffening results from a growth of W , yet, consistently, within $W \lesssim 200 \text{ mJ m}^{-2}$.

Since our rod bending data are consistent with the existence of a L -independent effective flexural modulus, we tentatively write k_0 as that of a beam of radius a_c (ref. ²⁷):

$$k_0 = \frac{12\pi E a_c^4}{a^3} = \frac{(3\pi)^{7/3} E}{4a^{1/3}} \left(\frac{W}{E^*}\right)^{4/3} \quad (4)$$

Since E and E^* are bulk properties that do not change over time, this expression suggests that the growth of k_0 arises from that of W . There is, indeed, clear evidence in the literature that, at room temperature, the interface between two silica surfaces ages, in particular by the formation of siloxanes^{41–45}. Yet, these studies support that siloxane formation results in a logarithmic growth of the total surface energy W , which includes van der Waals and chemical contributions. When combined with expression (4), this idea suggests that $k_0^{3/4}$ —not k_0 —grows logarithmically. Replotting our three-point bending data as $k_0^{3/4}$ versus t (Fig. 3d), we do find the logarithmic scaling to be more evident than in Fig. 3c as it now extends over two decades in time.

This remarkable scaling supports that contact ageing is akin to an increase over time of the total surface energy W between the

silica surfaces that causes a_c and thus k_0 to grow. Using our k_0 measurements together with expression (4), we estimate a_c to vary from 15 to 25 nm, small but not unreasonable values, while W grows from 30 to 200 mJ m^{-2} , a reasonable range³⁹.

Equation (4) predicts that the effective flexural rigidity depends on particle size only via the geometric prefactor $a^{-1/3}$. To test this scaling, we denote, from now on, $2a^* = 1.9 \mu\text{m}$ as the diameter of the particles used in the three-point bending test, and $k_0(a^*)$ the corresponding bending modulus. Combining equations (2) and (4) yields,

$$G' = S \frac{(a^*)^{1/3}}{a^{4/3}} k_0(a^*, t) \quad (5)$$

which predicts that, since $[k_0(a^*)]^{3/4}$, $(G')^{3/4}$ and not G' grows logarithmically in time. We check this eventuality by plotting (Fig. 1b) $(G')^{3/4}$ versus t , and find a visible enhancement of the scaling range.

To further test equation (5), we report in Fig. 4a, $G'(t)$ versus $k_0(a^*; t)$, for $a \neq a^*$, and systematically find a linear relation ($G' \simeq C + N k_0(a^*)$). The intercept C , occasionally non-zero, but always $< 50 \text{ kPa}$, appears to result from experimental errors. Indeed, (1) it is uncorrelated with our parameters (a , I or ϕ); (2) its values correspond to the indeterminacy of the origin of ageing time in either rheometry or flexural bending experiments and (3) to errors of less than 0.03 N m^{-1} on $k_0(a^*)$; that is, within our error bars. Using the fit parameters C, N , we reconstruct (see the brightly coloured symbols in Fig. 1) $G'(t)$ from the $k_0(a^*)$ time series: the excellent collapse shows macroscopic modulus ageing can be predicted using contact ageing data for a single particle size.

Next, for each suspension, we use slope N to estimate the structural parameter S of equation (5):

$$S \simeq \frac{a^{4/3}}{(a^*)^{1/3}} N \quad (6)$$

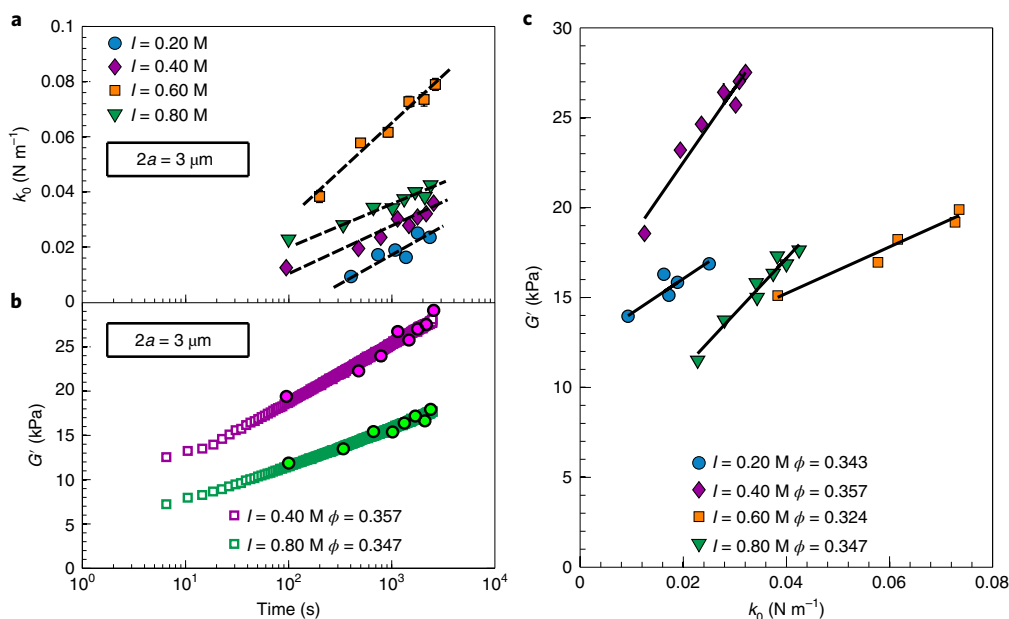


Fig. 5 | Macroscopic and contact ageing in PMMA suspensions. **a**, Time evolution of the bond stiffness for different salt concentrations I , measured with the three-point bending tests. **b**, Macroscopic shear modulus G' (coloured squares) for two suspensions with $\phi \simeq 0.35$ and different ionic strengths along with the modulus reconstructed from the k_0 time series (brightly coloured circles) using a linear fit as shown in the next panel. **c**, Shear modulus G' versus k_0 for the same ageing times, showing that the two quantities are well described by a linear relationship.

All these S values, when plotted versus ϕ (Fig. 4b) collapse on a single curve. It confirms experimentally our model prediction for the particle size scaling of G' , with the dimensionless prefactor S depending neither on particle size, nor on ionic strength. S rapidly increases with ϕ . The data suggest it diverges at a packing fraction ϕ_c , since they match reasonably well the form $S = S_0/(\phi_c - \phi)^\alpha$, for example, with $\phi_c \simeq 0.52$ and $\alpha = 4$, as shown. Such an $S(\phi)$ relation, when combined with equations (2) and (4), and with a logarithmic growth of W , provides a complete fit of our data set for varying I , ϕ , a and t .

Although these results are satisfactory, we remain surprised by, and cannot fully explain, the good agreement of our k_0 and G' data with the ageing law $\propto (\log(t/\tau))^{4/3}$, which emerges from our very simplified description of contacts. Thus, while we bring compelling experimental evidence that contact ageing drives macroscopic ageing (equation (5)), we emphasize that theoretical progress on the precise mechanism of contact ageing and on the link between contact rigidity and the modulus of particulate structures is still required.

A test of genericity

The core result of our work is the experimental demonstration that macroscopic mechanical ageing may arise solely from contact ageing, with the microstructure being fixed. We expect that it should be a widespread phenomenon, since it is likely to apply as soon as the formation of interparticle contacts cannot be prevented.

To test this expectation, we have examined PMMA suspensions in CaCl_2 salt solutions for a single particle size $2a = 3 \mu\text{m}$ and I values between 0.2 and 0.8 M. In all cases, we were again able to form stable rods (when held by their extremities). Moreover, in all studied cases, k_0 ages quasi-logarithmically (Fig. 5a).

These observations demonstrate the formation, between PMMA particles, of solid–solid contacts that age. Yet, in contrast with the case of silica particles, the bending stiffness (Fig. 5a) depends significantly and non-monotonically on I . This feature was previously noted by Pantina and Furst²⁸, who attributed it to a particle charge reversal resulting from the affinity of Ca^{2+} cations with the PMMA surface. Noticeably, for PMMA particles, contact ageing may be ascribed to the chain interdigitations occurring at the contact interface³², hence via a different mechanism from the case of silica.

Like k_0 , the macroscopic shear modulus of PMMA suspensions (Fig. 5b), is sensitive to ionic strength. To test equation (2), we report in Fig. 5c our $G'(t)$ versus $k_0(t)$ data for several ionic strengths. All of these plots are very clearly linear: $G' \simeq C + Nk_0$. However, in sharp contrast with the case of silica particle suspensions, the intercepts are large and cannot arise from experimental errors. It indicates that, at very early times, when the bending rigidity is negligibly small, PMMA suspensions already present an initial measurable macroscopic modulus $G'_0 \simeq C$ associated with the network of attractive interparticle bonds. The linearity of the G' versus k_0 plots supports that G' is just the sum of two contributions: G'_0 , which does not age, and Nk_0 , which does, due to contact ageing. Indeed, the growth of $G'(t)$ can be reconstructed from the $k_0(t)$ times series, using just the two fit parameters G'_0 and N : see the brightly coloured symbols in Fig. 5b, which fall right atop the $G'(t)$ curve. Our PMMA data thus demonstrate that, just as with silica suspensions, the growth of G' can be attributed to that of k_0 , irrespective of the value of the initial modulus G'_0 .

Contact-driven ageing

In this article, we have identified a single ageing scenario, in two concentrated, ionic, model suspensions with particles of sharply different natures. First, the microstructure rapidly stabilizes due to the formation of irreversible contacts; then, macroscopic shear-modulus ageing proceeds due to contact stiffening; that is, the growth of interparticle flexural rigidity.

It is noteworthy that our micrometre-sized silica particles could sediment over seconds if they were not interacting. Hence, the stability of our suspensions at moderate volume fractions (at least down to 33%, ref. 7) signals the rapid formation of attractive contacts. Besides, in both our systems, since rejuvenation is easily achieved by preshearing, solid–solid contacts, although stable under thermal fluctuations, break under moderate stresses. These observations underline that suspensions may be both homogeneous and easily reshuffled by shearing, even when particles form solid–solid contacts that are stable at rest. Stability and homogeneity hence may be facilitated by solid–solid contact formation.

The key condition for the relevance of our scenario is that the formation of solid–solid contacts is essentially not barrier limited:

that is significantly faster than other processes (diffusion, sedimentation). Indeed, typically, solid–solid contacts between micrometre-sized colloidal particles involve adhesion energies in the 1,000 kT range³², hence they cannot be opened by thermal activation at room temperature^{33,34}. So, at moderate or high packing fractions, such suspensions rapidly freeze into thermally irreversible structures. Additionally, (1) solid–solid contacts generically display roll-resistance⁴⁶, due to surface roughness and (2) contacts age under broad conditions, although via different routes depending on the physico-chemistries of the particles and suspending fluid.

For these reasons, our scenario of rapid stabilization by contact formation followed by contact-driven mechanical ageing is expected to arise as soon as the ionic concentration is sufficient to screen out Coulombic repulsion. This is probably the case in many materials of practical importance, such as cements at a young age²⁵, sediments, ceramics, sewage sludge, mine tailings and so on, which present ionic concentrations typically larger than those considered here. Whenever our scenario applies, the quantitative relations we have identified between contact and mechanical ageing provide a plausible starting point for predictive models.

The precise domain of relevance of our scenario, of course, will need to be assessed case-by-case. Contact ageing may also compete with structural ageing; for example, if the formation of contacts is not as rapid as here, that is limited by non-vanishing but small barriers, or if solid–solid contacts are weak enough to open by thermal activation. Progress on these questions will open the route towards the possibility to tune mechanical ageing by controlling and tailoring the surface chemistry of particles; a fascinating perspective in many applications.

Online content

Any methods, additional references, Nature Research reporting summaries, source data, extended data, supplementary information, acknowledgements, peer review information; details of author contributions and competing interests; and statements of data and code availability are available at <https://doi.org/10.1038/s41563-020-0624-9>.

Received: 11 December 2018; Accepted: 27 January 2020;

Published online: 02 March 2020

References

- Abou, B., Bonn, D. & Meunier, J. Aging dynamics in a colloidal glass. *Phys. Rev. E* **64**, 021510 (2001).
- Derec, C., Ducouret, G., Ajdari, A. & Lequeux, F. Aging and nonlinear rheology in suspensions of polyethylene oxide-protected silica particles. *Phys. Rev. E* **67**, 061403 (2003).
- Cousot, P., Tabuteau, H., Chateau, X., Tocquer, L. & Ovarlez, G. Aging and solid or liquid behavior in pastes. *J. Rheol.* **50**, 975–994 (2006).
- Ovarlez, G. & Coussot, P. Physical age of soft-jammed systems. *Phys. Rev. E* **76**, 011406 (2007).
- Ovarlez, G. & Chateau, X. Influence of shear stress applied during flow stoppage and rest period on the mechanical properties of thixotropic suspensions. *Phys. Rev. E* **77**, 061403 (2008).
- Guo, H., Ramakrishnan, S., Harden, J. L. & Leheny, R. L. Gel formation and aging in weakly attractive nanocolloid suspensions at intermediate concentrations. *J. Chem. Phys.* **135**, 154903 (2011).
- Fusier, J., Goyon, J., Chateau, X. & Toussaint, F. Rheology signature of flocculated silica suspensions. *J. Rheol.* **62**, 753–771 (2018).
- Dinsmore, A. D., Weeks, E. R., Prasad, V., Levitt, A. C. & Weitz, D. A. Three-dimensional confocal microscopy of colloids. *Appl. Opt.* **40**, 4152–4159 (2001).
- Dinsmore, A. D. & Weitz, D. A. Direct imaging of three-dimensional structure and topology of colloidal gels. *J. Phys. Cond. Matter* **14**, 7581–7597 (2002).
- Prasad, V., Semwogerere, D. & Weeks, E. R. Confocal microscopy of colloids. *J. Phys. Cond. Matter* **19**, 113102 (2007).
- Dibble, C. J., Kogan, M. & Solomon, M. J. Structure and dynamics of colloidal depletion gels: coincidence of transitions and heterogeneity. *Phys. Rev. E* **74**, 041403 (2006).
- Whitaker, K. A. et al. Colloidal gel elasticity arises from the packing of locally glassy clusters. *Nat. Commun.* **10**, 2237 (2019).

- Cipelletti, L., Manley, S., Ball, R. C. & Weitz, D. A. Universal aging features in the restructuring of fractal colloidal gels. *Phys. Rev. Lett.* **84**, 2275–2278 (2000).
- Bissig, H., Romer, S., Cipelletti, L., Trappe, V. & Schurtenberger, P. Intermittent dynamics and hyper-aging in dense colloidal gels. *Phys. Chem. Comm.* **6**, 21–23 (2003).
- Cipelletti, L. et al. Universal non-diffusive slow dynamics in aging soft matter. *Faraday Discuss.* **123**, 237–251 (2003).
- Barnes, H. A. Thixotropy: a review. *J. Nonnewton. Fluid Mech.* **70**, 1–33 (1997).
- Cipelletti, L. & Ramos, L. Slow dynamics in glassy soft matter. *J. Phys. Cond. Matter* **17**, R253 (2005).
- Mewis, J. & Wagner, N. J. *Colloidal Suspension Rheology* Cambridge Series in Chemical Engineering (Cambridge Univ. Press, 2011).
- Bouzid, M., Colombo, J., Barbosa, L. V. & Del Gado, E. Elastically driven intermittent microscopic dynamics in soft solids. *Nat. Commun.* **8**, 15846 (2017).
- Dieterich, J. H. & Kilgore, B. D. Imaging surface contacts: power law contact distributions and contact stresses in quartz, calcite, glass and acrylic plastic. *Tectonophysics* **256**, 219–239 (1996).
- Persson, B. N. J. *Sliding Friction: Physical Principles and Applications* (Springer, 2000).
- Baumberger, T. & Caroli, C. Solid friction from stick-slip down to pinning and aging. *Adv. Phys.* **55**, 279–348 (2006).
- Vandamme, M. & Ulm, F.-J. Nanogranular origin of concrete creep. *Proc. Natl Acad. Sci. USA* **106**, 10552–10557 (2009).
- Ioannidou, K. et al. The crucial effect of early-stage gelation on the mechanical properties of cement hydrates. *Nat. Commun.* **7**, 12106 (2016).
- Roussel, N., Ovarlez, G., Garrault, S. & Brumaud, C. The origins of thixotropy of fresh cement pastes. *Cement Concrete Res.* **42**, 148–157 (2012).
- Manley, S. et al. Time-dependent strength of colloidal gels. *Phys. Rev. Lett.* **95**, 048302 (2005).
- Pantina, J. P. & Furst, E. M. Elasticity and critical bending moment of model colloidal aggregates. *Phys. Rev. Lett.* **94**, 138301 (2005).
- Pantina, J. P. & Furst, E. M. Colloidal aggregate micromechanics in the presence of divalent ions. *Langmuir* **22**, 5282–5288 (2006).
- Meng, B., Wu, J., Li, Y. & Lou, L. Aging process of the bond between colloidal particles measured using laser tweezers. *Colloids Surf. A* **322**, 253–255 (2008).
- Buscall, R., Mills, P. D. A., Goodwin, J. W. & Lawson, D. W. Scaling behaviour of the rheology of aggregate networks formed from colloidal particles. *J. Chem. Soc., Faraday Trans.* **84**, 4249–4260 (1988).
- Russel, W. B., Saville, D. A. & Schowalter, W. R. *Colloidal Dispersions* Cambridge Monographs on Mechanics (Cambridge Univ. Press, 1989).
- Israelachvili, J. N. in *Intermolecular and Surface Forces* 3rd edn (ed. Israelachvili, J. N.) 415–467 (Academic Press, 2011).
- Swan, J. W., Shindel, M. M. & Furst, E. M. Measuring thermal rupture force distributions from an ensemble of trajectories. *Phys. Rev. Lett.* **109**, 198302 (2012).
- Whitaker, K. A. & Furst, E. M. Bond rupture between colloidal particles with a depletion interaction. *J. Rheol.* **60**, 517–529 (2016).
- Derjaguin, B., Muller, V. & Toporov, Y. Effect of contact deformations on the adhesion of particles. *J. Colloid Interface Sci.* **53**, 314–326 (1975).
- Johnson, K. L., Kendall, K. & Roberts, A. D. Surface energy and the contact of elastic solids. *Proc. R. Soc. London A* **324**, 301–313 (1971).
- Tabor, D. Surface forces and surface interactions. *J. Colloid Interface Sci.* **58**, 2–13 (1977).
- Paul, J., Romeis, S., Tomas, J. & Peukert, W. A review of models for single particle compression and their application to silica microspheres. *Adv. Powder Technol.* **25**, 136–153 (2014).
- Iler, K. *The Chemistry of Silica: Solubility, Polymerization, Colloid and Surface Properties and Biochemistry of Silica* (John Wiley & Sons, Inc., 1979).
- Guleryuz, H., Røyset, A. K., Kaus, I., Filiâtre, C. & Einarsrud, M.-A. Afm measurements of forces between silica surfaces. *J. Sol-Gel Sci. Techn.* **62**, 460–469 (2012).
- Vigil, G., Xu, Z., Steinberg, S. & Israelachvili, J. Interactions of silica surfaces. *J. Colloid Interface Sci.* **165**, 367–385 (1994).
- Li, Q., Tullis, T. E., Goldsby, D. & Carpick, R. W. Frictional ageing from interfacial bonding and the origins of rate and state friction. *Nature* **480**, 233 EP (2011).
- Liu, Y. & Szlufarska, I. Chemical origins of frictional aging. *Phys. Rev. Lett.* **109**, 186102 (2012).
- Tian, K. et al. Load and time dependence of interfacial chemical bond-induced friction at the nanoscale. *Phys. Rev. Lett.* **118**, 076103 (2017).
- Li, Z., Pastewka, L. & Szlufarska, I. Chemical aging of large-scale randomly rough frictional contacts. *Phys. Rev. E* **98**, 023001 (2018).
- DelGado, E. & Kob, W. A microscopic model for colloidal gels with directional effective interactions: network induced glassy dynamics. *Soft Matter* **6**, 1547–1558 (2010).

Publisher's note Springer Nature remains neutral with regard to jurisdictional claims in published maps and institutional affiliations.

© The Author(s), under exclusive licence to Springer Nature Limited 2020

Methods

Particles. Silica micro particles were produced by a single growth step Stöber synthesis⁴⁷ in a semibatch process (continuous addition). This is considered to be the best method to ensure sphericity and monodispersity⁴⁸. We added small amounts of electrolyte (NaCl, Sigma-Aldrich) to the initial ammonia solution, at concentrations ranging from 1 to 4 mM, to achieve better control of the final particle size⁴⁹. Particles were separated by centrifugation and then washed several times with ethanol 96% (GPR Rectapur VWR) and with deionized water (Aquadem 18 M Ω) to eliminate impurities and solvents. They were finally dried at 60 °C for several days.

The particle sizes in all batches (for both rheometry and bending test) were measured by dynamic light scattering (Malvern Zetasizer Nano S). In addition, we collected scanning electron microscopy micrographs (Zeiss Neon 40 EsB FIB-SEM) of the particles used in laser-tweezer experiments to have more accurate size measurements; we found them to present a mean diameter $d = 1,860 \pm 90$ nm and 5% polydispersity, which compares well with the dynamic light scattering results ($d = 1,960 \pm 420$ nm).

PMMA particles were purchased from MicroBeads (Spheromers CA3). Particle sizes were distributed around 3 μm with a 15% polydispersity. The particles were washed several times with ethanol and deionized water before use.

Suspensions. Suspensions were prepared following the protocol shown by Fusier et al.⁷ to permit experimental reproducibility. A small amount of dry silica powder (of known weight) was dispersed and left for several hours in a large volume of deionized water; the mixture was then centrifuged at 5,000 r.p.m. for 5 min to eliminate the gross part of water; salt was dissolved in the volume of water needed to reach the target packing fraction ϕ and ionic strength I ; finally, the centrifuged particles and saline water were vigorously mixed until a homogeneous suspension was obtained.

A slightly different procedure was required for PMMA suspensions, as the hydrophobicity of the PMMA surface⁵⁰ complicated the dispersion process. Dispersed PMMA particles were stirred for two days and then allowed to sediment overnight; most of the excess water along with some hydrophobic particles adsorbed at the air–liquid interface had to be removed using a syringe. Centrifugation was performed at 5,500 r.p.m. for 20 min.

Rheometry. Rheology was performed using a stress-controlled (Malvern Kinexus Ultra +) rheometer, in a thin (1.25-mm) gap Couette geometry between roughened cylinders to avoid slippage. After the rheometer cup was filled, sonification was performed for 2 min to remove bubbles.

Before each measurement, the system was presheared at 200 s⁻¹ for 3 min, a high strain-rate corresponding to two to three times the yield stress⁷. This brought our suspensions into a well-defined initial state, and ensured the reproducibility of the ensuing shear-modulus evolution⁷. The end of preshear was taken as the origin of ageing time.

The shear modulus was then measured at different times by applying an oscillatory shear stress at 1 Hz (to avoid retro-action noise), using a feedback loop to achieve a strain amplitude of 10⁻⁴, and thus stay within the linear regime⁷.

Confocal microscopy. We used a confocal microscope (Zeiss LSM 700) with a $\times 100$ numerical aperture 1.4 oil immersion objective (Zeiss Plan-APOCHROMAT). We imaged silica particles in a 60/40 wt% mixture of water/glycerol with a small amount of fluorescein. Our confocal microscopy measurements were performed in a single focal plane, at a depth of around 15 μm . The acquisition time of an image (0.5 s) was short compared with our observation timescale. Particle reconstruction was performed using a standard centroid-based algorithm⁵¹. This permitted the positioning of particles within a tenth of a pixel, which corresponds to around 12 nm in our two-dimensional snapshots^{51,52}. However, due to the residual index mismatch our resolution was slightly lower.

Bending test. We used the custom-made tweezers setup in ref. ⁵³ that permitted us to manipulate multiple particles by time-sharing a single laser beam (see details in the referenced paper). Before each experiment, the trap stiffness, k_{trap} , was measured by examining the thermal fluctuations of a trapped bead, the position of which is resolved with nanometric accuracy by back-focal plane interferometry⁵⁴. The sample cells were made using a double-sided adhesive spacer to create a gap between a microscope slide (Fisher, size 25 \times 75 \times 1 mm³) and a coverslip (Fisher, size 22 \times 30 \times 0.17 mm³).

We studied beams formed using a single particle size $2a = 1.9$ μm . This choice resulted from a compromise between two constraints: (1) the higher the a , the broader the range of accessible forces (set by the silica/water optical index contrast⁵⁵) and the better the evaluation of particle positions at subpixel accuracy; and (2) it is difficult to synthesize large monodisperse particles. The chosen a value limited polydispersity to 5%, while allowing us to access the desired rod properties.

A difficulty we encountered was that, at the targeted salt concentrations, both SiO₂ and PMMA particles, which sedimented due to density contrast, stuck so strongly to the coverslip that they could not be detached with the tweezers. To

manipulate these particles, we needed to postpone the time when particles entered the saline solution. We achieved this by dividing the cell into two compartments carved in the adhesive spacer: a small (7 μl) one, where a highly diluted ($\phi \approx 10^{-4}$) suspension of particles in pure water was introduced and a large one (50 μl), where the solution was introduced. To prevent drying, the whole cell was sealed using a fast UV-curing epoxy (Norland Products, NOA 81) immediately after the introduction of the ionic solution and suspended particles. The two compartments were in open contact with each other through a small aperture, which sufficiently slowed down salt diffusion so that particles, although they did sediment, did not stick to the coverslip and could be handled for nearly 2 h. The size difference between the two compartments guaranteed that even after the complete diffusive dispersion of salt, the relative error in the ionic strength remained smaller than around 5%.

We used beams of 11 or 13 particles. They were assembled using an array of the same number of time-shared traps separated by a distance (around 2.5 μm) larger than the particle diameter. The array was filled with particles inside the small compartment and then moved through the aperture to the ionic solution (large compartment) by means of the motorized microscope stage. The beam was finally formed by reducing the separation between the traps until van der Waals forces induced aggregation²⁷.

The full aggregation of a beam took roughly 1 min due to fluctuations caused primarily by Brownian motion. The formation of the last contact was taken as the origin of time for the beam evolution. Thereafter, the beam was held only by three traps: two at its extremities, and one at its centre. Bending was enforced by translating the centre trap perpendicular to the chain at a velocity slow enough to create negligible hydrodynamic drag (30 nm s⁻¹), while the two other traps were fixed. We called x the axis passing through the end particles of the rod, and y the perpendicular axis in the focal plane of the microscope (see Fig. 3a). Microscope images, with a pixel size of 0.117 μm , provided particle positions at a subpixel (1/10th) precision of roughly 10 nm (ref. ⁵¹).

The trap stiffnesses being known, the bending force f was obtained from the y displacements of the end particles away from their preloading positions, which corresponded to the location of the (fixed) traps; the deflection was estimated as the differences in y of the end and central particles. The raw data thus inferred from y displacements alone, however, had to be corrected to take into account two main problems: (1) rods were not strictly linear and (2) the optical traps and microscope focal planes were not perfectly aligned. In Supplementary Methods, we explain how we did this and improve our measurements of f and δ .

Data availability

Figure source data are provided online; other data used in this work are available from the authors.

Code availability

The software used in this work is available from the authors.

References

- Stober, W., Fink, A. & Bohn, E. Controlled growth of monodisperse silica spheres in the micron size range. *J. Colloid Interface Sci.* **26**, 62–69 (1968).
- Do, K. K. & Taik, K. H. New process for the preparation of monodispersed, spherical silica particles. *J. Am. Ceram. Soc.* **85**, 1107–1113 (2002).
- Nakabayashi, H. et al. Electrolyte-added one-pot synthesis for producing monodisperse, micrometer-sized silica particles up to 7 μm . *Langmuir* **26**, 7512–7515 (2010).
- Laxton, P. B. & Berg, J. C. Investigation of the link between micromechanical interparticle bond rigidity measurements and macroscopic shear moduli of colloidal gels. *Colloids Surfaces A*. **301**, 137–140 (2007).
- Crocker, J. C. & Grier, D. G. Methods of digital video microscopy for colloidal studies. *J. Colloid Interface Sci.* **179**, 298–310 (1996).
- Gao, Y. X. & Kilfoil, M. L. Accurate detection and complete tracking of large populations of features in three dimensions. *Optics Expr.* **17**, 4685–4704 (2009).
- Pantina, J. P. & Furst, E. M. Directed assembly and rupture mechanics of colloidal aggregates. *Langmuir* **20**, 3940–3946 (2004).
- Shindel, M. M., Swan, J. W. & Furst, E. M. Calibration of an optical tweezer microrheometer by sequential impulse response. *Rheologica Acta* **52**, 455–465 (2013).
- Niemenen, T. A., Knöner, G., Heckenberg, N. R. & Rubinsztein-Dunlop, H. in *Laser Manipulation of Cells and Tissues, Methods in Cell Biology* Vol. 82 (eds Berns, M. W. & Greulich, K. O.) 207–236 (Academic Press, 2007).

Acknowledgements

This work benefited from a French government grant managed by ANR within the framework of the National Program Investments for the Future, ANR-11-LABX-0022-01. F.B.'s stay at the University of Delaware was supported by University Paris-Est.

Author contributions

X.C., J.G. and A.L. conceived and supervised the project. J.G. and J.F. designed the macroscopic shear-modulus ageing protocol and obtained data on silica suspensions. J.G. supervised sample preparation and all experiments. E.M.F. designed the laser tweezer three-point flexural test and supervised its use. F.B. obtained complementary macroscopic shear modulus data, designed the two-compartment cell, performed flexural ageing measurements with E.M.F. and J.G. All authors contributed to the interpretation of experimental data, model construction and article planning and writing.

Competing interests

The authors declare no competing interests.

Additional information

Supplementary information is available for this paper at <https://doi.org/10.1038/s41563-020-0624-9>.

Correspondence and requests for materials should be addressed to X.C. or A.L.

Reprints and permissions information is available at www.nature.com/reprints.